Two-step charge density wave transition and hidden transient phase in 1T-TiSe$_2$

R. Amin [1], J. Pandey [1,2] K. Beyer [3], and V. Petkov [1,*]

[1]*Department of Physics, Central Michigan University, Mt. Pleasant, Michigan 48859, USA*
[2]*Department of Chemistry, Faculty of Science, SGT University, Gurugram, Haryana 122505, India*
[3]*X-ray Science Division, Advanced Photon Source, Argonne National Laboratory, Illinois 60439, USA*

Using variable temperature atomic pair distribution function analysis, we study the emergence of charge density wave (CDW) order in 1T-TiSe$_2$ and find that it takes place via a two-step transition. First, upon decreasing temperature to about 235(3) K, CDW-related lattice distortions emerge in the individual TiSe$_2$ layers alone. Then, upon further decreasing the temperature, the two-dimensional distortions in the layers couple and the widely recognized three-dimensional $2a_0 \times 2a_0 \times 2c_0$ superstructure emerges at about 205(3) K. Because two different band gaps are known to emerge at the same temperatures, the finding indicates the presence of strong electron-phonon coupling. The transient phase between the two steps lacks inversion symmetry and may serve as a precursor of the debated chiral 1T-TiSe$_2$ phase. Our findings are important for the understanding of the enigmatic CDW transition in 1T-TiSe$_2$ and CDW instabilities in van der Waals materials in general.

I. INTRODUCTION

The transition metal dichalcogenide (TMD) 1T-TiSe$_2$ exhibits rich physics due to its quasi-two-dimensional (2D) structure and interactions between its electronic and lattice degrees of freedom [1–11]. It is made of weakly interacting layers of Ti-Se$_6$ octahedra [Fig. 1(a)] that are stacked along the c axis of a structure with a centrosymmetric space group (SG) $P\bar{3}m1$ symmetry. Upon decreasing temperature, commensurate charge density wave (CDW) order emerges at $T_{CDW(3D)}$ of 205(3) K, the band gap increases, and 1T-TiSe$_2$ adopts a $2a_0 \times 2a_0 \times 2c_0$ superstructure with a centrosymmetric SG $P\bar{3}c1$ symmetry [12,13]. In the superstructure, Ti and Se atoms appear displaced from their position in the high-temperature, undistorted phase as shown in Figs. 1(e) and 1(f). Despite the intense effort, the mechanism of the CDW transition in 1T-TiSe$_2$ remains a hotly debated topic because, contrary to many CDW systems from the TMDs family, it does not appear to be driven by Fermi-surface (FS) nesting or saddle-point singularities, as parallel FS sheets have neither been predicted [14] nor observed [15–17]. It has been proposed that a driving force for the transition is the Jahn-Teller effect, where the energy is lowered, and charge modulation emerges because of lattice distortions [16,18–20]. Some authors have suggested that the CDW transition is due to an exitonic condensation, which triggers lattice distortions [11,21,22], while others argued that it is driven by strong electron-phonon interactions. Coupled exciton and phonon interactions have also been suggested as a driving force for the transition [18–23]. Furthermore, it has been suggested that CDW 1T-TiSe$_2$ has chiral character [24,25]. While the discovery of static chirality in 1T-TiSe$_2$ has been questioned in later studies [26–28], the possible emergence of

a chiral 1T-TiSe$_2$ phase induced by external stimuli such as photoexcitations has not been ruled out [10]. The contradictions are further magnified by the failure of traditional Bragg scattering experiments conducted so far to clearly reveal the structural changes taking place during the CDW transition. This is because such experiments do not consider the diffuse scattering component in the experimental data [12], thereby disregarding the presence of local structural disorder that smears fine features of the CDW transition in 1T-TiSe$_2$. On the other hand, prior diffuse scattering experiments successfully revealed the presence of soft phonon modes in 1T-TiSe$_2$ [2,23], but did not consider the Bragg component of the experimental data, thereby providing limited information about the complex temperature evolution of the static lattice distortions in 1T-TiSe$_2$. To fill the knowledge gap and resolve the contradictions, we study 1T-TiSe$_2$ by atomic pair distribution function (PDF) analysis over a broad temperature range, including the CDW transition. The technique considers both the diffuse and the Bragg scattering components in the diffraction data and has proven useful in structural studies of materials exhibiting lattice distortions, including CDW phases of TMDs [29–32]. We find that the CDW order emerges from an environment that includes preexisting local lattice distortions, underlining the importance of the crystal lattice to the emergence of electronic order in 1T-TiSe$_2$. We also find that the CDW transition proceeds in two steps. First, upon decreasing temperature to $T_{CDW(2D)} = 235(3)$ K, the material suffers a lattice distortion confined to the individual Ti-Se$_6$ layers. Then, the distortions in the individual layers couple, and three-dimensional (3D) CDW order emerges at $T_{CDW(3D)} = 205(3)$ K. Because of the presence of strong rms atomic displacements, i.e., dynamic structural disorder, the phase boundaries between the undistorted $a_0 \times a_0 \times c_0$, transient 2D ($2a_0 \times 2a_0$) and fully evolved 3D ($2a_0 \times 2a_0 \times 2c_0$) CDW structures appear smeared, which may explain the observed variation in the reported $T_{CDW(3D)}$ values [26,28]. Our study resolves

*petko1vg@cmich.edu

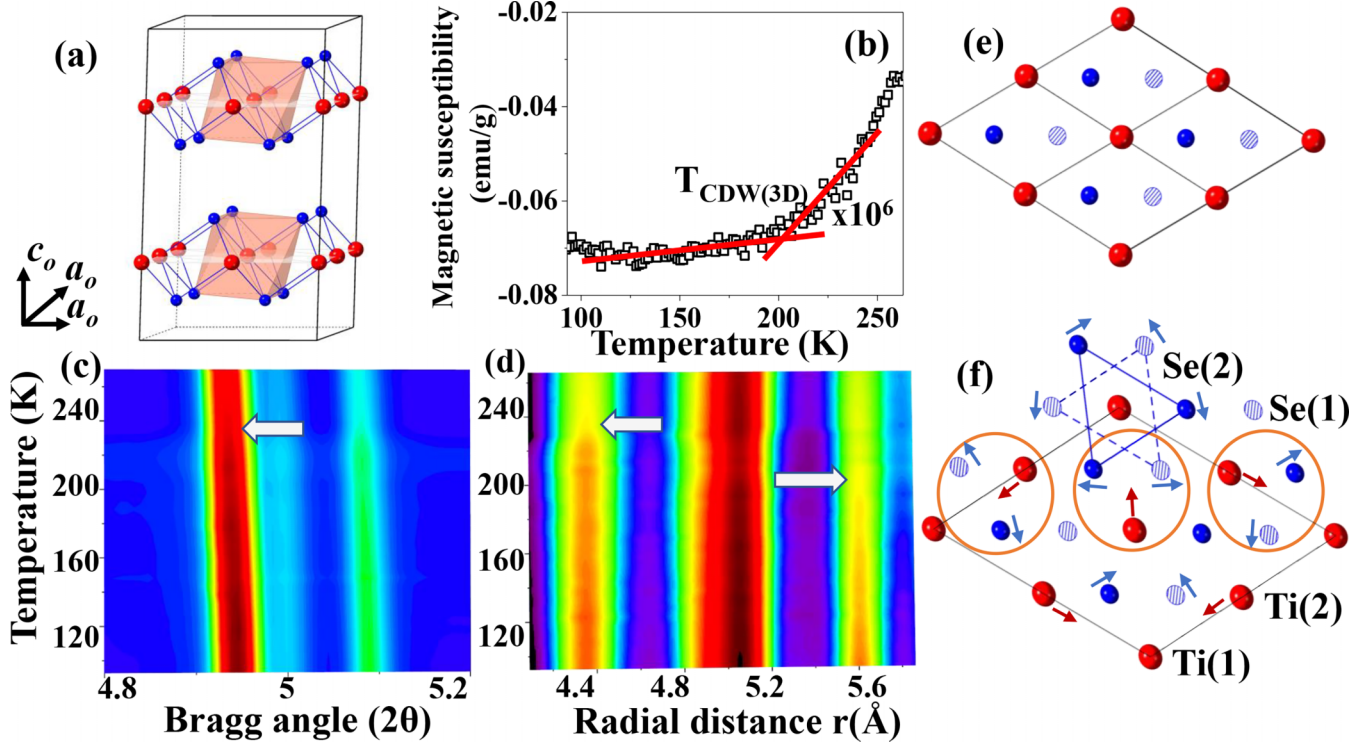FIG. 1. (a) $2a_0 \times 2a_0 \times 2c_0$ supercell for $1T$-TiSe$_2$ (outlined) including layers of Ti-Se$_6$ octahedra. Ti atoms are in red and Se atoms in blue. (b) Temperature evolution of the magnetic susceptibility for TiSe$_2$ indicating the presence of a broad phase transition at about $T_{CDW(3D)} = 205(3)$ K. Intensity color maps of selected peaks in (c) XRD patterns and (d) atomic PDFs for $1T$-TiSe$_2$. Arrows indicate changes in PDF peak intensities close to $T_{CDW(3D)} = 205(3)$ K and $T_{CDW(2D)} = 235(3)$ K. Projection of a Se-Ti-Se layer in (e) undistorted $1T$-TiSe$_2$ and (f) CDW $1T$-TiSe$_2$ on a basal Ti plane. Blue and red arrows indicate the direction of the in-plane static displacements of, respectively, Se and Ti atoms during the CDW transition. Dark and light blue circles show Se(1) and Se(2) atoms positioned above and below the basal Ti plane, respectively. Ti(1), Ti(2), Se(1) and Se(2) occupy positions (0,0,0.25), (0.58,0,0.25), (0.3333, 0.6667, 0.1225) and (0.3333, 0.195, 0.1225) in the SG $P\bar{3}c1$ structure.

the controversies about the nature of the CDW transition in $1T$-TiSe$_2$ and calls for similar studies on the variety of CDW orders exhibited by TMDs and other strongly correlated van der Waals systems [33–37].

II. EXPERIMENT

A. Sample preparation and characterization

A high-quality $1T$-TiSe$_2$ sample was provided by 2D semiconductors [38]. In-house x-ray diffraction (XRD) measurements showed that it is phase pure and exhibits a trigonal (SG $P\bar{3}m1$) structure. To illustrate the effect of CDW transition on the electronic properties, we measured the temperature evolution of the magnetization using a physical property measuring system from Quantum Design. Experimental data are shown in Fig. 1(b). In line with earlier results [12], the magnetic susceptibility, χ, appears small, on the order of 10^{-8} emu/g, because its paramagnetic and diamagnetic components are comparable in magnitude. The rate of change of χ with temperature is seen to gradually decrease near 205(3) K, reflecting the sluggish nature of the CDW transition.

B. Synchrotron x-ray radiation experiments

Using synchrotron x rays with energy of 105.7 keV ($\lambda = 0.1173$ Å), XRD data were collected at the beamline 11-ID-C

at the Advanced Photon Source, Argonne National Laboratory, over a temperature range from 263 to 93 K in steps of 5 K. The sample temperature was controlled using a Linkam thermal stage and the scattered intensities were collected with a 2D detector. Two sets of XRD patterns were collected at each temperature. One of the patterns was collected with the detector positioned 1500 mm away from the sample to achieve high resolution in reciprocal space. The patterns were used to perform Rietveld analysis. The other set of patterns was collected with the detector positioned 300 mm away from the sample to reach wave vector, q, values as high as 30 Å^{-1}. The patterns were used to derive atomic PDFs using procedures described in [39,40]. Intensity color maps for the XRD patterns collected to high q values and atomic PDFs derived from them are shown in Figs. 1(c) and 1(d). Intensity variations are clearly seen for temperatures in the range from 200 to 240 K.

III. STRUCTURE MODELING

To investigate the average crystal structure in more detail, the high-q resolution synchrotron XRD data were subjected to Rietveld analysis [41]. As an example, Rietveld fits to XRD patterns collected at 263 and 93 K are shown in Supplemental material Fig. S1 [42]. The 263 K data set is fit better with a model exhibiting a trigonal SG $P\bar{3}m1$ type structure in comparison to the supercell SG $P\bar{3}c1$ model. The opposite
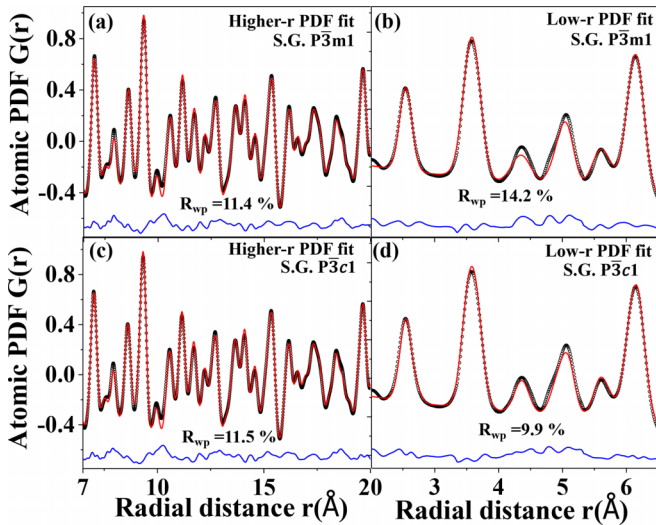
FIG. 2. (a),(b) Fits (red line) to the high- and low-r parts of the experimental PDF (symbols) for 1T-TiSe$_2$ obtained at 263 K. The fits are based on a SG $P\bar{3}m1$-type model. (c),(d) Fits to the high- and low-r parts of the same experimental PDF based on a SG $P\bar{3}c1$-type model. The residual difference (blue line) is shifted for clarity. The agreement factor R_{wp} is given for each fit. The refined supercell (SG $P\bar{3}c1$) model does not outperform the refined undistorted model (SG $P\bar{3}m1$) in the higher-r PDF region (c) vs (a). The opposite is true for the low-r PDF data (d) vs (b).

is true for the 93 K data set. The results confirm that, at low temperature, a long-range $2a_0 \times 2a_0 \times 2c_0$ superstructure emerges in 1T-TiSe$_2$.

Fits to PDF data obtained at 263 K are shown in Fig. 2. The higher-r PDF data [Fig. 2(a)], which have an increased sensitivity to the average crystal structure in comparison to the low-r PDF data, are fit well with the undistorted (SG $P\bar{3}m1$) structure model. However, the low-r PDF data, in particular the 4.5 and 5 Å PDF peaks reflecting interlayer atomic correlations (Fig. S2 in [42]), are fit better with the supercell (SG $P\bar{3}c1$) model in comparison to the undistorted (SG $P\bar{3}m1$) model [compare the PDF fits in Figs. 2(b) and 2(d)], where, in addition to the large anisotropic thermal factors, small static displacements of Ti, Δ(Ti) = 0.04(1) Å, and Se, Δ(Se) = 0.02(1) Å, atoms from their positions in the undistorted lattice are allowed to occur. The result indicates that the crystal lattice of 1T-TiSe$_2$ experiences local lattice distortions related to CDW order at temperatures well above $T_{\mathrm{CDW(3D)}}$.

Fits to PDF data obtained at 93 K are shown in Fig. 3. The PDF data cannot be fit well with the SG $P\bar{3}c1$ model [Figs. 3(a) and 3(c)] unless the highly anisotropic in-plane u_{11}, u_{22} rms displacements for Ti atoms are decoupled and refined independently from the u_{12} rms displacements [Figs. 3(b) and 3(d)]. The result indicates that, locally, CDW 1T-TiSe$_2$ keeps experiencing highly anisotropic structural disorder at temperatures well below $T_{\mathrm{CDW(3D)}}$. Earlier neutron diffraction studies [20] have indicated that a model featuring a Ti-displacement pattern leading to Ti-Se distances as short as 2.4 Å is more successful in describing the local structure in CDW 1T-TiSe$_2$ in comparison to the widely accepted SG $P\bar{3}c1$ model. However, similarly to other high-energy XRD
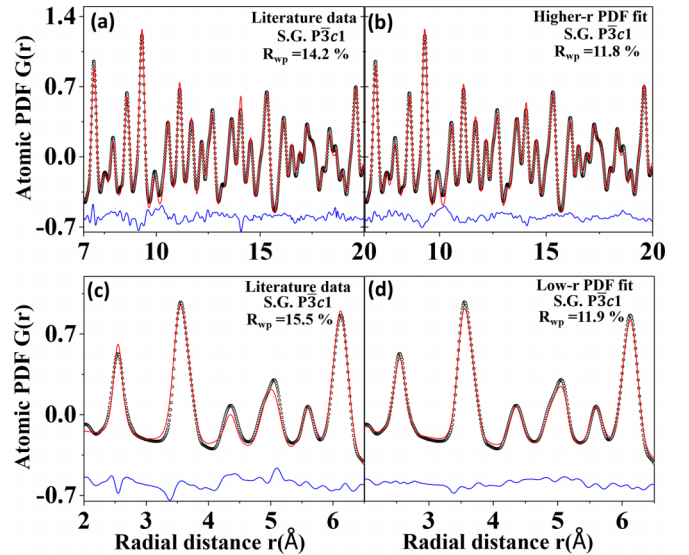

FIG. 3. (a),(c) Comparison between PDF computed from literature data (red) and experimental PDF (black) obtained at 93 K. Fits (red) to the same experimental PDF (black) data, including both highly anisotropic rms and static atomic displacements. In addition, in the fits, the u_{12} rms displacement of Ti(1) atoms is decoupled from the u_{11} and u_{22} rms ones. For reference, $u_{11} = u_{22}$ and $u_{12} = 0.5u_{11}$ in the SG $P\bar{3}c1$ structure models. The residual difference (blue line) is shifted for clarity. The agreement factor R_{wp} is given for each data set.
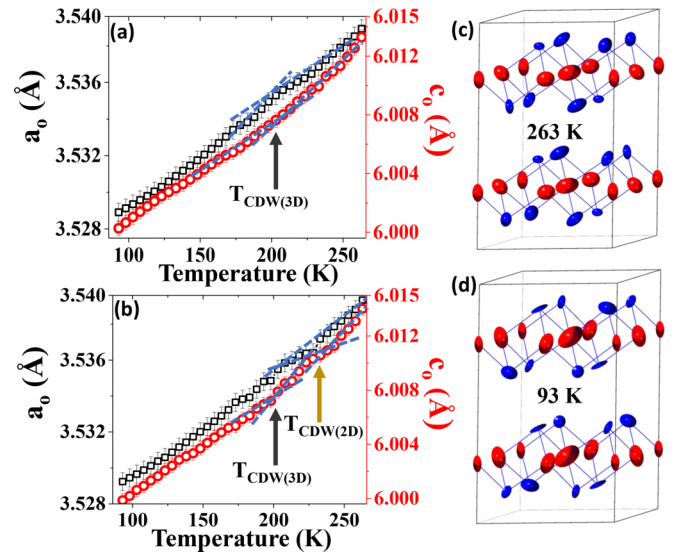

FIG. 4. (a) Rietveld and (b) PDF refined a_0 and c_0 lattice parameters for 1T-TiSe$_2$ as a function of temperature. The thermal evolution of the Rietveld refined parameters shows a departure from linearity (follow the blue dotted lines) with an inflection point close to $T_{\mathrm{CDW(3D)}}$ = 205(3) K. That for the PDF refined a_0 and c_0 lattice parameters shows a departure from linearity with inflection points close to $T_{\mathrm{CDW(3D)}}$ = 205(3) K and $T_{\mathrm{CDW(2D)}}$ = 235(3) K (follow the blue dotted lines). (c),(d) Local view of the crystal structure of the undistorted (263 K) and CDW (93 K) phase of 1T-TiSe$_2$ with the rms displacements of the atoms shown. The structure in (c) reflects the fit to the PDF data obtained at 263 K [Fig. 2(d)]. The crystal structure in (d) reflects the fit to the PDF data obtained at 93 K [Fig. 3(d)].
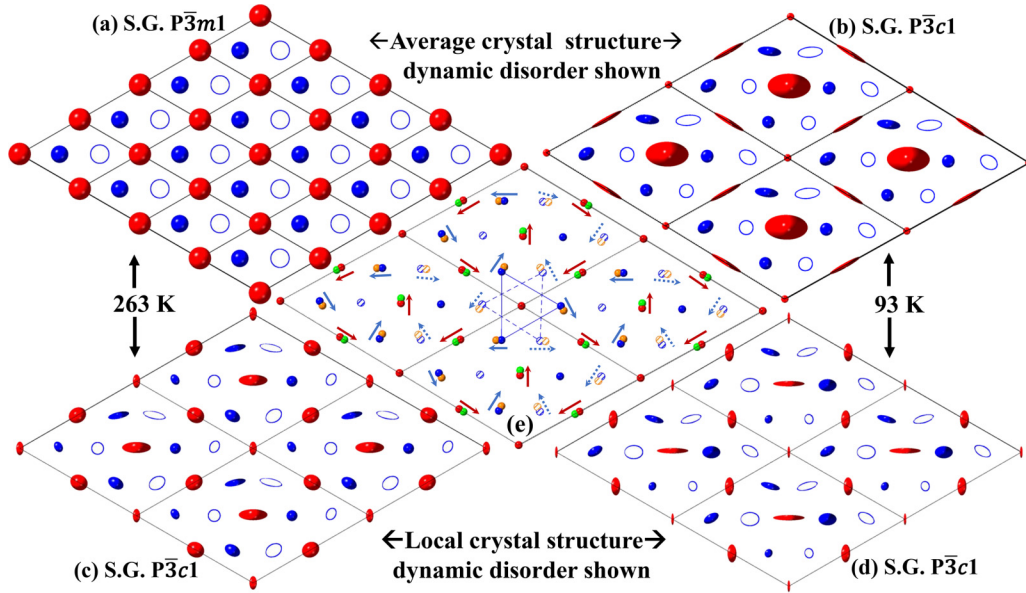
FIG. 5. (a) Projection of a single Se-Ti-Se layer in $1T$-TiSe$_2$ (263 K) onto a Ti plane, as derived from a fit [Fig. 2(a)] to high-r PDF data. (b) Projection of a single Se-Ti-Se layer in CDW $1T$-TiSe$_2$ (93 K) onto a Ti plane, as derived from a fit [Fig. 3(b)] to high-r PDF data. (c) Projection of a Se-Ti-Se layer in $1T$-TiSe$_2$ (263 K) onto a Ti plane, as derived from a fit [Fig. 2(d)] to low-r PDF data. (d) Projection of a Se-Ti-Se layer in CDW $1T$-TiSe$_2$ (93 K) onto a Ti plane, as derived from a fit [Fig. 3(d)] to low-r PDF data. (e) Schematics of the in-plane static displacements/rotations (follow the arrows) of Ti(2) and Se(2) atoms during the CDW transition. Ti atoms are in red. Se atoms above and below the Ti plane are in dark and light blue, respectively.

studies [43], the first peak in the atomic PDFs obtained here appears rather symmetric in shape (Fig. S2 in [42]), indicating that the bonding distances in $1T$-TiSe$_2$ do not change dramatically when the CDW order emerges. In particular, at 93 K, the maximum static displacements of Ti and Se atoms amount to 0.06(1) and 0.03(1) Å, respectively, when derived from fits to high-r PDF data. These values are close to the previously published results [12,43,44]. The displacements appear slightly larger, 0.07(1) and 0.04(1) Å, respectively, when derived from fits to low-r PDF data. A local view of the crystal structure of the undistorted and CDW phase of $1T$-TiSe$_2$, emphasizing the presence of highly anisotropic rms displacements in both phases, is shown in Figs. 4(c) and 4(d). Also shown in the figure is the temperature evolution of the Rietveld and PDF refined values for the lattice parameters of $1T$-TiSe$_2$. The former shows a departure from linearity with an inflection point close to $T_{\mathrm{CDW}} = 205(3)$ K. The latter shows a departure from linearity with inflection points close to $T_{\mathrm{CDW(3D)}} = 205(3)$ K and $T_{\mathrm{CDW(2D)}} = 235(3)$ K. The nonlinearity extends over a temperature range from about 170 to 240 K, reflecting the presence of an overall lattice instability in this temperature region. Projections of the average and local structure of $1T$-TiSe$_2$ at 263 K (non-CDW phase) and 93 K (3D CDW phase) on a single Ti plane are shown in Fig. 5, as derived by fits to high- and low-r PDF data, respectively. The temperature evolution of the static and rms atomic displacements of Ti and Se atoms in $1T$-TiSe$_2$ is shown in Fig. 6.

IV. DISCUSSION

A. Mechanism of the CDW transition

As can be seen in Figs. 6(a) and 6(b), upon decreasing temperature, Ti(2) and Se(2) atoms experience in-plane

static displacements at a temperature of $T_{\mathrm{CDW(2D)}} = 235(3)$ K, where Se(2) atoms above and below the Ti plane rotate in opposite directions. The out-of-plane static displacement of the atoms is negligible. By contrast, Se(1) atoms start experiencing out-of-plane static displacements at $T_{\mathrm{CDW(3D)}} = 205(3)$ K, while their in-plane static displacement is negligible. Evidently, the CDW phase transition in $1T$-TiSe$_2$ is a two-step process that proceeds through a transient phase existing over a temperature range from $T_{\mathrm{CDW(2D)}}$ to $T_{\mathrm{CDW(3D)}}$ [~30(6) K wide]. That is, upon cooling down to $T_{\mathrm{CDW(2D)}}$, static lattice distortions related to CDW order emerge only in the individual Ti-Se$_2$ layers. Upon further cooling down to $T_{\mathrm{CDW(3D)}}$, a static CDW modulation in the z direction of the crystal lattice develops and 3D CDW order sets in. The presence of two steps in the CDW phase transition in $1T$-TiSe$_2$ is also seen in the thermal evolution of PDF refined lattice parameters shown in Fig. 4(b). Interestingly, the thermal evolutions of the in- and out-of-plane rms displacements of Ti(1) atoms [Fig. 6(c)], which do not undergo static displacements during the CDW transition, also exhibit nonlinearities close to $T_{\mathrm{CDW(2D)}}$ and $T_{\mathrm{CDW(3D)}}$. The nonlinearity of the thermal evolution of the rms displacements of Ti(2) atoms, which undergo static displacements during the CDW transition, is less well expressed [Fig. 6(e)]. Notably, the thermal evolution of the rms displacements of Se(1) and Se(2) atoms [Figs. 6(d) and 6(f)] appears flat in the vicinity of both $T_{\mathrm{CDW(2D)}}$ and $T_{\mathrm{CDW(3D)}}$, but becomes highly nonlinear below $T^* \sim 170$ K, where a broad peak in the resistivity is often observed [45–48]. It is likely that the significantly increased in- and out-of-plane rms displacements of Se(2) atoms and in-plane displacements (u_{22}) of Se(1) atoms observed below T^*, i.e., dynamic structural disorder, is at least partially responsible for this peak.
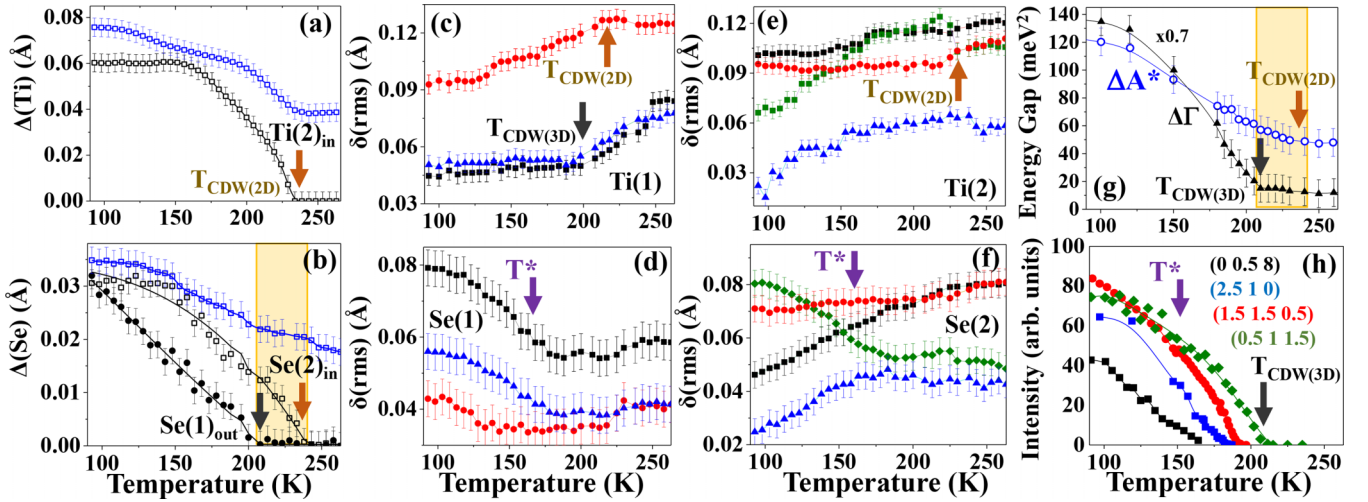
FIG. 6. (a),(b) Temperature evolution of the average (black) and local (blue) static displacements of Ti(2), Se(1), and Se(2) atoms from their position in the undistorted lattice. (c)–(f) Temperature evolution of the rms displacements, u_{ij} (black), u_{22} (green), u_{12} (blue), and u_{33} (red) for Ti and Se atoms. (g) Square of the experimental energy band gaps $\Delta\Gamma$ and ΔA^* as a function of temperature. Because the $2a_0 \times 2a_0 \times 2c_0$ lattice modulation involves a coupling between Γ and L [53], $\Delta\Gamma$ may be expected to exhibit an onset at $T_{CDW(3D)}$ determined here, which is exactly what data for $\Delta\Gamma$ in (g) show. On the other hand, as discussed in Ref. [53], the gap ΔA^* involves both the $2a_0 \times 2a_0 \times 2c_0$ and $2a_0 \times 2a_0 \times 1c_0$ lattice modulations, but the dominant effect comes from the latter, and, accordingly, the ΔA^* onset may be expected to appear at $T_{CDW(2D)}$ determined here, which is exactly what data for ΔA^* in (g) show. (h) Integrated intensity of observed superlattice reflections [26,28]. Black arrows in the plots point to $T_{CDW(3D)} = 205(3)$ K where at 3D CDW order emerges in $1T$-TiSe$_2$. Brown arrows in the plots point to $T_{CDW(2D)} = 235(3)$ K where at 2D CDW-like order emerges in the individual Ti-Se$_2$ planes. Purple arrows in the plots point to a temperature $T^* \sim 170$ K where at the rms displacements of Se(1) and Se(2) atoms show a pronounced nonlinearity and an anomalous increase in the resistivity is observed [44]. Light-brown rectangles in (b) and (g) outline the boundaries of the transient phase.

Plotted in Fig. 6(h) is the temperature evolution of the intensity of superlattice reflections measured by single-crystal experiments [26,28,49]. The evolution of (0.5,1,1.5) and (1.5,1.5,0.5) peaks resembles that of the in-plane static displacements of Ti(2) and Se(2) atoms [Fig. 6(a)]. On the other hand, the evolution of (2.5,1,0) and (0,0.5,8) peaks resembles that of the out-of-plane static displacements of Se(1) atoms [Fig. 6(d)]. Furthermore, the temperatures whereat the peaks are seen to decay to zero appear scattered over a broad temperature range extending between T^* and $T_{CDW(3D)}$. Then, it appears that the debated differences [28] in the decay of different superlattice peaks with temperature merely reflect the fact that different families of superlattice peaks are sensitive to different types of atomic displacements [26], which, in turn, vary widely in amplitude and temperature evolution below $T_{CDW(3D)}$ (see Fig. 6). Furthermore, it also becomes evident that, essentially, due to the incomplete 3D CDW order and large dynamic disorder, the transient 2D CDW order emerging between $T_{CDW(2D)}$ and $T_{CDW(3D)}$ would be hard to detect using traditional techniques based on an analysis of sharp Bragg peaks alone. However, as demonstrated here, it is possible to be detected using atomic PDF analysis, which considers both the Bragg and the diffuse scattering components in the diffraction data in real space [39].

B. Electron-lattice interaction

In its normal state, $1T$-TiSe$_2$ is a narrow band gap semiconductor, where the Se $4p$ valence-band maximum is at the Γ point and the Ti $3d$ conduction-band minimum is at the L point of the Brillouin zone. Studies have shown that the CDW

transition leads to band folding and gap renormalization. In particular, the Γ and L points appear significantly repelled from the Fermi energy, and the valence-band maximum shifts to the A point [45,49–52]. To explore the relationship between the emerging lattice distortions and changes in the electronic structure taking place during the CDW transition, in Fig. 6(g) we plot experimental data for the energy band gaps $\Delta\Gamma$ and ΔA^* between, respectively, Γ and L and A^* and L points as a function of temperature [53]. The data show that $\Delta\Gamma$ and ΔA^* increase as the temperature decreases, but the onset temperature of their increase is different. The onset of ΔA^* appears close to $T_{CDW(2D)}$ while that of $\Delta\Gamma$ appears close to $T_{CDW(3D)}$. The result indicates that both the emergence of CDW-related periodic lattice distortions and renormalization of different band gaps is a two-step transition, where the respective transition temperatures are nearly identical, attesting to the presence of a strong electron-phonon coupling in $1T$-TiSe$_2$ [23,54].

C. Transient CDW state and chiral order

The phonon dispersion for $1T$-TiSe$_2$ is known to exhibit two soft modes, one at the L and the other at the M point. It also exhibits a strong anharmonicity in the vicinity of the CDW transition [23,55], which likely reflects the highly anisotropic nature of the rms displacement of Ti and Se atoms (see Figs. 5 and 6). The soft mode at the L point corresponds to a $2a_0 \times 2a_0 \times 2c_0$ lattice reconstruction while that at the M point corresponds to a $2a_0 \times 2a_0 \times 1c_0$ lattice reconstruction. As our PDF result shows, upon decreasing temperature, the $2a_0 \times 2a_0 \times 1c_0$ lattice reconstruction involving in-plane static atomic displacements [rotations; see Fig. 5(e)], i.e.,

softening the M phonon mode, takes place at $T_{CDW(2D)}$. Because atomic displacements/rotations in different layers are effectively decoupled, they may not necessarily appear related by inversion symmetry, as they are in the $2a_0 \times 2a_0 \times 2c_0$ superstructure with centrosymmetric (achiral) SG $P\bar{3}c1$ symmetry that emerges when the L phonon mode also softens and 3D CDW order emerges at $T_{CDW(3D)}$. Hence, transient domains of CDWs fluctuating [56–58] in terms of chirality may emerge in the temperature range between $T_{CDW(2D)}$ and $T_{CDW(3D)}$. Depending on the thermal prehistory of the sample and/or application of specific external stimuli, chiral CDW domains may grow and stabilize below $T_{CDW(3D)}$ at the expense of nonchiral CDW domains, eventually leading to the emergence of a more-or-less complete chiral CDW order [59–62]. As shown in numerous studies, however, under normal thermodynamic conditions, achiral CDW order tends to set in below $T_{CDW(3D)}$ [1–6,12–18,41,46–48].

D. Dimensionality effect on the CDW transition

Reducing the physical dimensions of TMDs down to a few layers may be expected to affect the CDW order they exhibit because of the weakening of the interlayer interactions and reduced electronic screening. In the monolayer (ML) limit, $1T$-type TMDs involving Se such as $1T$-NbSe$_2$ and $1T$-TaSe$_2$ have been found to exhibit strongly enhanced CDW order, where the temperature at which it sets in, $T_{CDW(ML)}$, is higher than $T_{CDW(3D)}$ in the respective bulk material [63,64]. For example, while in bulk $1T$-NbSe$_2$ the CDW order sets in at $T_{CDW(3D)} = 33.5$ K, the CDW transition in a $1T$-NbSe$_2$ monolayer takes place at $T_{CDW(ML)} = 145$ K. Single-layer $1T$-VSe$_2$ has also been reported to exhibit strongly enhanced CDW order, where $T_{CDW(ML)} = 220$ K is nearly twice the bulk value of $T_{CDW(3D)} = 110$ K. Contrary to the case of $1T$-NbSe$_2$, however, the CDW periodicity in a $1T$-VSe$_2$ monolayer appears different from that of the layers in bulk $1T$-VSe$_2$ [65]. It has been reported that a supported $1T$-TiSe$_2$ monolayer preserves the $2a_0 \times 2a_0$ CDW periodicity of the stacked layers in bulk $1T$-TiSe$_2$ and, furthermore, exhibits CDW order below $T_{CDW(ML)} = 232(5)$ K [44,53,66], which is the same as $T_{CDW(2D)}$ for the stacked layers forming bulk $1T$-TiSe$_2$. The picture that emerges from our study is that each layer in bulk $1T$-TiSe$_2$ develops a $2a_0 \times 2a_0$ lattice modulation independently at $T_{CDW(2D)}$, which is also the CDW transition temperature $T_{CDW(ML)}$ for a $1T$-TiSe$_2$ monolayer. At the lower transition temperature $T_{CDW(3D)}$, the $2a_0 \times 2a_0$ modulated $1T$-TiSe$_2$ layers merely lock their 2D structure into a $2a_0 \times 2a_0 \times 2c_0$ superstructure, accompanied by an anisotropic band gap increase.

V. CONCLUSION

We find that $1T$-TiSe$_2$ suffers significant local structural disorder well above the CDW transition, including both static and rms atomic displacements of Ti and Se atoms from their position in the (on average) centrosymmetric SG $P\bar{3}m1$ crystal lattice. Upon decreasing temperature, $1T$-TiSe$_2$ undergoes a two-step phase transition. At first, 2D CDW-like order emerges in the individual Ti-Se$_2$ layers alone and the material loses its inversion symmetry, providing an opportunity for the emergence of chiral CDW order. Due to strong dynamic structural disorder, this 2D CDW order remains "hidden" for traditional crystallography.

Upon further decreasing the temperature, achiral 3D CDW order emerges, where the average crystallographic structure attains centrosymmetric SG $P\bar{3}c1$ symmetry. The results shed extra light on the mechanism of the enigmatic CDW transition in $1T$-TiSe$_2$ and are likely to help achieve a comprehensive understanding of charge ordering phenomena in TMDs, in particular, and van der Waals materials, in general.

[1] J. A. Wilson, F. J. Di Salvo, and S. Mahajan, Charge-density waves and superlattices in the metallic layered transition metal dichalcogenides, Adv. Phys. **24**, 117 (1975).

[2] M. Holt, P. Zschack, H. Hong, M. Y. Chou, and T.-C. Chiang, X-ray studies of phonon softening in TiSe$_2$, Phys. Rev. Lett. **86**, 3799 (2001).

[3] S. Manzeli, D. Ovchinnikov, D. Pasquier, O. V. Yazyev, and A. Kis, 2D transition metal dichalcogenides, Nat. Rev. Mater. **2**, 17033 (2017).

[4] M. Calandra and F. Mauri, Charge-density wave and superconducting dome in TiSe$_2$ from electron-phonon interaction, Phys. Rev. Lett. **106**, 196406 (2011).

[5] S. Mathias *et al.*, Self-amplified photo-induced gap quenching in a correlated electron material, Nat. Commun. **7**, 12902 (2016).

[6] D. Pasquier and O. V. Yazyev, Excitonic effects in two-dimensional TiSe$_2$ from hybrid density functional theory, Phys. Rev. B **98**, 235106 (2018).

[7] E. Morosan, H. W. Zandbergen, B. S. Dennis, J. W. G. Bos, Y. Onose, T. Klimczuk, A. P. Ramirez, N. P. Ong, and R. J. Cava, Superconductivity in Cu$_x$TiSe$_2$, Nat. Phys. **2**, 544 (2006).

[8] Y. Liu, R. Ang, W. J. Lu, W. H. Song, L. J. Li, and Y. P. Sun, Superconductivity induced by Se-doping in layered charge-density-wave system $1T$-TaS$_{2-x}$Se$_x$, Appl. Phys. Lett. **102**, 192602 (2013).

[9] M. M. May, C. Brabetz, C. Janowitz, and R. Manzke, Charge-density-wave phase of $1T$-TiSe$_2$: The influence of conduction band population, Phys. Rev. Lett. **107**, 176405 (2011).

[10] S. Y. Xu, Q. Ma, Y. Gao, A. Kogar, A. Zong, A. M. Valdivia, T. H. Dinh, S. M. Huang, B. Singh, C. H. Hsu, T. R. Chang, J.

P. C. Ruff, K. Watanabe, T. Taniguchi, H. Lin, G. Karapetrov, D. Xiao, P. J. Herrero, and N. Gedik, Spontaneous gyrotropic electronic order in a transition-metal dichalcogenide, Nature (London) **578**, 545 (2020).

[11] A. Kogar, M. S. Rak, S. Vig, A. A. Husain, F. Flicker, Y. I. Joe, L. Venema, G. J. Macdougall, T. C. Chiang, E. Fradkin, J. V. Wezel, and P. Abbamonte, Signatures of exciton condensation in a transition metal dichalcogenide, Science **358**, 1314 (2017).

[12] F. J. Di Salvo, D. E. Moncton, and J. V. Waszczak, Electronic properties and superlattice formation in the semimetal $TiSe_2$, Phys. Rev. B **14**, 4321 (1976).

[13] J. A. Wilson, Concerning the semimetallic characters of TiS_2 and $TiSe_2$, Solid State Commun. **22**, 551 (1977).

[14] A. Zunger and A. J. Freeman, Band structure and lattice instability of $TiSe_2$, Phys. Rev. B **17**, 1839 (1978).

[15] O. Anderson, R. Manzke, and M. Skibowski, Three-dimensional and relativistic effects in layered $1T$-$TiSe_2$, Phys. Rev. Lett. **55**, 2188 (1985).

[16] T. E. Kidd, T. Miller, M. Y. Chou, and T.-C. Chiang, Electron-hole coupling and the charge density wave transition in $TiSe_2$, Phys. Rev. Lett. **88**, 226402 (2002).

[17] D. Qian, D. Hsieh, L. Wray, E. Morosan, N. L. Wang, Y. Xia, R. J. Cava, and M. Z. Hasan, Emergence of Fermi pockets in a new excitonic charge-density-wave melted superconductor, Phys. Rev. Lett. **98**, 117007 (2007).

[18] H. P. Hughes, Structural distortion in $TiSe_2$ and related materials—a possible Jahn-Teller effect? J. Phys. C: Solid State Phys. **10**, L319 (1977).

[19] M. H. Whangbo and E. Canadell, Analogies between the concepts of molecular chemistry and solid-state physics concerning structural instabilities. Electronic origin of the structural modulations in layered transition metal dichalcogenides, J. Am. Chem. Soc. **114**, 9587 (1992).

[20] A. Wegner, J. Zhao, J. Li, J. Yang, A. A. Anikin, G. Karapetrov, K. Esfarjani, D. Louca, and U. Chatterjee, Evidence for pseudo–Jahn-Teller distortions in the charge density wave phase of $1T$-$TiSe_2$, Phys. Rev. B **101**, 195145 (2020).

[21] C. S. Snow, J. F. Karpus, S. L. Cooper, T. E. Kidd, and T.-C. Chiang, Quantum melting of the charge-density-wave state in $1T$-$TiSe_2$, Phys. Rev. Lett. **91**, 136402 (2003).

[22] E. Möhr-Vorobeva, S. L. Johnson, P. Beaud, U. Staub, R. De Souza, C. Milne, G. Ingold, J. Demsar, H. Schaefer, and A. Titov, Nonthermal melting of a charge density wave in $TiSe_2$, Phys. Rev. Lett. **107**, 036403 (2011).

[23] F. Weber, S. Rosenkranz, J.-P. Castellan, R. Osborn, G. Karapetrov, R. Hott, R. Heid, K.-P. Bohnen, and A. Alatas, Electron-phonon coupling and the soft phonon mode in $TiSe_2$, Phys. Rev. Lett. **107**, 266401 (2011).

[24] J. Van Wezel, P. Nahai-Williamson, and S. S. Saxena, Exciton-phonon-driven charge density wave in $TiSe_2$, Phys. Rev. B **81**, 165109 (2010).

[25] B. Zenker, H. Fehske, H. Beck, C. Monney, and A. R. Bishop, Chiral charge order in $1T$-$TiSe_2$: Importance of lattice degrees of freedom, Phys. Rev. B **88**, 075138 (2013).

[26] H. Ueda, M. Porer, J. R. L. Mardegan, S. Parchenko, N. Gurung, F. Fabrizi, M. Ramakrishnan, L. Boie, M. J. Neugebauer, B. Burganov, M. Burian, S. L. Johnson, K. Rossnagel, and U.

Staub, Correlation between electronic and structural orders in $1T$-$TiSe_2$, Phys. Rev. Res. **3**, L022003 (2021).

[27] C. W. Chuang, Y. Tanaka, M. Oura, K. Rossnagel, and A. Chainani, Attractive Coulomb interaction, temperature-dependent hybridization, and natural circular dichroism in $1T$-$TiSe_2$, Phys. Rev. B **102**, 195102 (2020).

[28] M.-K. Lin, J. A. Hlevyack, P. Chen, R.-Y. Liu, and T.-C. Chiang, Comment on "Chiral phase transition in charge ordered $1T$-$TiSe_2$" Phys. Rev. Lett. **122**, 229701 (2019).

[29] A. Wegner, D. Louca, and J. Yang, Local trigonal modes and the suppression of the charge density wave in $TiSe_{2-x}Te_x$, Phys. Rev. B **99**, 205110 (2019).

[30] V. Petkov, K. Chapagain, J. Yang, S. Shastri, and Y. Ren, Exotic bonding interactions and coexistence of chemically distinct periodic lattice distortions in the charge density wave compound $TaTe_2$, Phys. Rev. B **102**, 024111 (2020).

[31] V. Petkov, K. Chapagain, S. Shastri, and Y. Ren, Genesis of the periodic lattice distortions in the charge density wave state of $2H$-$TaSe_2$, Phys. Rev. B **101**, 121114(R) (2020).

[32] E. S. Bozin, M. Abeykoon, S. Conradson, G. Baldinozzi, P. Sutar, and D. Mihailovic, Crystallization of polarons through charge and spin ordering transitions in $1T$-TaS_2, Nat. Commun. **14**, 7055 (2023).

[33] X. Teng *et al.*, Discovery of charge density wave in a kagome lattice antiferromagnet, Nature (London) **609**, 490 (2022).

[34] Y. Wang, D. F. Agterberg, and A. Chubukov, Coexistence of charge-density-wave and pair-density-wave orders in underdoped cuprates, Phys. Rev. Lett. **114**, 197001 (2015).

[35] J. R. Neilson, T. M. McQueen, A. Llobet, J. Wen, and M. R. Suchomel, Charge density wave fluctuations, heavy electrons, and superconductivity in KNi_2S_2, Phys. Rev. B **87**, 045124 (2013).

[36] J. Chang, E. Blackburn, A. T. Holmes, N. B. Christensen, J. Larsen, J. Mesot, R. Liang, D. A. Bonn, W. N. Hardy, A. Watenphul, M. v. Zimmermann, E. M. Forgan, and S. M. Hayden, Direct observation of competition between superconductivity and charge density wave order in $YBa_2Cu_3O_{6.67}$, Nat. Phys. **8**, 871 (2012).

[37] M. Leroux, V. Mishra, C. Opagiste, P. Rodière, A. Kayani, W.-K. Kwok, and U. Welp, Charge density wave and superconductivity competition in $Lu_5Ir_4Si_{10}$: A proton irradiation study, Phys. Rev. B **102**, 094519 (2020).

[38] Titanium Diselenide ($TiSe_2$), https://2dsemiconductors. com/TiSe2-Crystal/.

[39] H. P. Klug and L. E. Alexander, *X-Ray Diffraction Procedures for Polycrystalline and Amorphous Materials* (Wiley, New York, 1974).

[40] V. Petkov, *RAD*, a program for analysis of X-ray diffraction data from amorphous materials for personal computers, J. Appl. Crystallogr. **22**, 387 (1989).

[41] B. H. Toby and R. B. Von Dreele, *GSAS-II*: The genesis of a modern open-source all purpose crystallography software package, J. Appl. Crystallogr. **46**, 544 (2013).

[42] See Supplemental Material at http://link.aps.org/supplemental/ 10.1103/PhysRevB.109.144106 for Rietveld fits and atomic PDF data.

[43] P. K. Hamilton, J. M. Moya, A. M. Hallas, E. Morosan, R. Baral, and B. A. Frandsen, Symmetry-mode analysis for local

structure investigations using pair distribution function data, J. Appl. Crystallogr. **56**, 1192 (2023).

[44] X.-Y. Fang, H. Hong, P. Chen, and T.-C. Chiang, X-ray study of the charge-density-wave transition in single-layer TiSe$_2$, Phys. Rev. B **95**, 201409(R) (2017).

[45] K. Rossnagel, L. Kipp, and M. Skibowski, Charge-density-wave phase transition in 1T-TiSe$_2$: Excitonic insulator versus band-type Jahn-Teller mechanism, Phys. Rev. B **65**, 235101 (2002).

[46] J. M. Moya, C.-L. Huang, J. Choe, G. Costin, M. S. Foster, and E. Morosan, Effect of synthesis conditions on the electrical resistivity of TiSe$_2$, Phys. Rev. Mater. **3**, 084005 (2019).

[47] K. Rossnagel, On the origin of charge-density waves in select layered transition-metal dichalcogenides, J. Phys.: Condens. Matter **23**, 213001 (2011).

[48] M. D. Watson, A. M. Beales, and P. D. C. King, On the origin of the anomalous peak in the resistivity of TiSe$_2$, Phys. Rev. B **99**, 195142 (2019).

[49] Y. Peng, X. Guo, Q. Xiao, Q. Li, J. Strempfer, Y. Choi, D. Yan, H. Luo, Y. Huang, S. Jia, O. Janson, P. Abbamonte, J. van den Brink, and J. van Wenzel, Observation of orbital order in the van der Waals material 1T-TiSe$_2$, Phys. Rev. Res. **4**, 033053 (2022).

[50] R. Bianco, M. Calandra, and F. Mauri, Electronic and vibrational properties of TiSe$_2$ in the charge-density-wave phase from first principles, Phys. Rev. B **92**, 094107 (2015).

[51] G. Li, W. Z. Hu, D. Qian, D. Hsieh, M. Z. Hasan, E. Morosan, R. J. Cava, and N. L. Wang, Semimetal-to-semimetal charge density wave transition in 1T-TiSe$_2$, Phys. Rev. Lett. **99**, 027404 (2007).

[52] M. D. Watson, O. J. Clark, F. Mazzola, I. Marković, V. Sunko, T. K. Kim, K. Rossnagel, and P. D. C. King, Orbital- and k_z-selective hybridization of Se 4p and Ti 3d states in the charge density wave phase of TiSe$_2$, Phys. Rev. Lett. **122**, 076404 (2019).

[53] P. Chen, Y.-H. Chan, X.-Y. Fang, S.-K. Mo, Z. Hussain, A.-V. Fedorov, M. Y. Chou, and T.-C. Chiang, Hidden order and dimensional crossover of the charge density waves in TiSe$_2$, Sci. Rep. **6**, 37910 (2016).

[54] M. R. Otto, J.-H. Pöhls, L. P. René de Cotret, M. J. Stern, M. Sutton, and B. J. Siwick, Mechanisms of electron-phonon coupling unraveled in momentum and time: The case of soft phonons in TiSe$_2$, Sci. Adv. **7**, eabf2810 (2021).

[55] M. Hellgren, J. Baima, R. Bianco, M. Calandra, F. Mauri, and L. Wirtz, Critical role of the exchange interactions for the electronic structure and CDW formation in TiSe$_2$, Phys. Rev. Lett. **119**, 176401 (2017).

[56] P. Monceau, Electronic crystals: An experimental overview, Adv. Phys. **61**, 325 (2012).

[57] Q. Chen, D. Chen, W. Schnelle, C. Felser, and B. D. Gaulin, Charge density wave order and fluctuations above T_{CDW} and below superconducting T_c in the kagome metal CsV$_3$Sb$_5$, Phys. Rev. Lett. **129**, 056401 (2022).

[58] R. Arpaia, S. Caprara, R. Fumagalli, G. De Vecchi, Y. Y. Peng, E. Andersson, D. Betto, G. M. DeLuca, N. B. Brookes, F. Lombardi, M. Saluzzo, L. Braicovich, C. Di Castro, M. Grilli, and G. Ghiringhelli, Dynamical charge density fluctuations pervading the phase diagram of a Cu-based high-T_c superconductor, Science **365**, 906 (2019).

[59] D. Wickramaratne, S. Subedi, D. H. Torchinsky, G. Karapetrov, and I. I. Mazin, Photoinduced chiral charge density wave in TiSe$_2$, Phys. Rev. B **105**, 054102 (2022).

[60] J.-P. Castellan, S. Rosenkranz, R. Osborn, Q. Li, K. E. Gray, X. Luo, U. Welp, G. Karapetrov, J. P. C. Ruff, and J. Van Wezel, Chiral phase transition in charge ordered 1T-TiSe$_2$, Phys. Rev. Lett. **110**, 196404 (2013).

[61] J. Ishioka, Y. H. Liu, K. Shimatake, T. Kurosawa, K. Ichimura, Y. Toda, M. Oda, and S. Tanda, Chiral charge-density waves, Phys. Rev. Lett. **105**, 176401 (2010).

[62] J. Ishioka, T. Fujii, K. Katono, K. Ichimura, T. Kurosawa, M. Oda, and S. Tanda, Charge-parity symmetry observed through Friedel oscillations in chiral charge-density waves, Phys. Rev. B **84**, 245125 (2011).

[63] Y. Nakata, K. Sugawara, A. Chainani, H. Oka, C. Bao, S. Zhou, P.-Y. Chuang, C.-M. Cheng, T. Kawakami, Y. Saruta, T. Fukumura, S. Zhou, T. Takahashi, and T. Sato, Robust charge-density wave strengthened by electron correlations in monolayer 1T-TaSe$_2$ and 1T-NbSe$_2$, Nat. Commun. **12**, 5873 (2021).

[64] X. Xi, L. Zhao, Z. Wang, H. Berger, L. Forro, J. Shan, and K. F. Mak, Strongly enhanced CDW order in monolayer NbSe$_2$, Nat. Nanotechnol. **10**, 765 (2015).

[65] P. Chen, W. W. Pai, Y. Chan, V. Madhavan, M. Y. Chou, S. Mo, A. Fedorov, and T. Chiang, Unique gap structure and symmetry of the CDW in single-layer VSe$_2$, Phys. Rev. Lett. **121**, 196402 (2018).

[66] P. Chen, Y. Chan, X. Fang, Y. X. Zhang, M. Chou, S. Mo, A. Fedorov Z. Hussain, and T. Chiang, Charge density wave transition in single-layer titanium diselenide, Nat. Commun. **6**, 8943 (2015).